# Adjustable Power Modulation for a Leg Mechanism Suitable for Running

Mark Plecnik[1], Katherine Fearing[2], and Ronald S. Fearing[2]

*Abstract*— **Recent work in the design of mechanical systems for terrestrial locomotion has indicated successful strategies for increasing the energetic performance of a robotic locomotor without upgrading its actuator system. We apply one such strategy, termed power modulation, in a new way: for the design of a leg mechanism useful for running. Power modulation geometrically defines force/torque ratios between robot components to mechanically achieve certain energy transmission characteristics during fast stance dynamics that increase the kinetic power output of the overall system. Furthermore, we investigate the design of a leg mechanism that can adjust to exhibit power modulation. In this way, a leg mechanism would exhibit a low power mode for flat terrain, and can adjust to a high power mode for rough terrain. The latter makes jumping possible and extends the range of available footholds that can be accessed in a single step. To find a suitable leg mechanism, we leverage the Finite Root Generation method to compute a design. The design is advanced to a prototype and basic experiments are conducted to investigate its behavior as adjusted between high- and low-power modes.**

## I. INTRODUCTION

Research in legged robots is often motivated by the capability of accessing difficult terrains. By selecting discrete footholds, terrain might be traversed more safely, efficiently, quickly, or satisfy some other optimality metric. The set of available footholds from step to step is fundamentally constrained by power density. That is, footholds existing outside the direct workspace of a robot require a leaping or bounding motion defined by a finite propulsive moment of ground contact when ballistic energy might be generated.

Mechanical power output during stance is fundamentally limited by actuator selection for a rigidly connected system. Connecting an actuator in series with a spring to a leg mechanism allows for more complex power transmission between actuator, spring, and load. Creating a system to exploit these complexities to increase power transmission to the load presents a formidable design challenge. One approach, termed *series-elastic power modulation* [1], designs a variable mechanical advantage linkage. Mechanical advantage geometrically defines the ratio between an output and input force/torque during stance time dynamics. Carefully defining this ratio as a function of leg stroke allows for planned power transmission between actuator, spring, and load to automatically occur during fast dynamics.

In [2], this power modulating behavior was instantiated into the kinematic design of a monopedal jumping robot, Salto. In this work, we explore the design of this behavior into a limb useful for running and walking motions. To accomplish this, we append a few new requirements. First, the path of the foot must traverse the entirety of a closed mechanism circuit such that a motor continually rotating in the forward direction produces a periodic modulated stance phase. Second, the path must allow for ground clearance as the foot recycles back for its next stance phase. And last, we desire some adjustability in the mechanism geometry so that power modulating behavior can be switched on and off. In this way, a robot traversing simple, flat terrain may adjust to use low-powered, efficient mechanics. High-powered mechanics are reserved for rough terrain.

Recent research on energetic design principles for legged locomotion focuses on the advantages of direct drive robots [3], [4]. Small hexapedal runners have also pushed the limits of high speed running [5] and can even be outfitted with adaptations to traverse obstacles by jumping [6] or accomplishing intricate cooperation primitives [7]. Paluska and Herr [8] analyzed energetic implications of series elasticity for robotic applications. De and Koditschek [9] explored energizing spring legs with a tail for hopping. The RHex robot [10] incorporates springy legs to accomplish dynamic motions. Yesilevskiy et al. [11] analyzed the implications of parallel-elastic and series-elastic actuation on energy efficiency.

We present a series-elastic leg design that more directly exploits mechanism geometry to achieve greater energetics. This design is found computationally by the Finite Root Generation technique [12], detailed in Section II. The construction of a prototype and test methods are described in Section III. Finally, test results are analyzed in Section IV and conclusions offered in Section V.

## II. DESIGN

### A. Required Behaviors

Our leg mechanism exhibits the following required behaviors:

1) Kinetic power output during stance phase multiples the motor's power limit (power modulation).
2) The mechanism traverses a full circuit of configurations with its input rotating in the forward direction.

*This work was supported by National Science Foundation award CMMI-1636302. Any opinions, findings, and conclusions or recommendations expressed in this material are those of the authors and do not necessarily reflect the views of the National Science Foundation.

[1]Mark Plecnik is a postdoctoral scholar in the Biomimetic Millisystems at the University of California, Berkeley mplecnik@berkeley.edu

[2]Katherine Fearing is a student in the Department of Mechanical Engineering at the University of California, Berkeley kfearing@berkeley.edu

[3]Ronald S. Fearing is a professor in the Department of Electrical Engineering and Computer Science at the University of California, Berkeley ronf@eecs.berkeley.edu

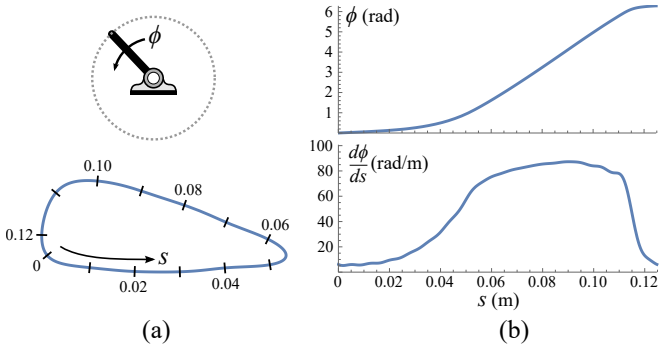


Fig. 1. (a) Kinematic synthesis of a timed curve generator involves designing a coupler point path and coordinating it with an input link at the same time. (b) The derivative of the coordinating function between input crank angle and path arc length is equal to mechanical advantage.

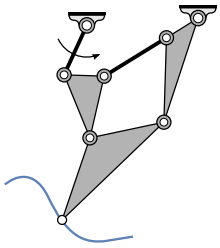

Fig. 2. A planar six-bar linkage is proposed for coordinating a coupler path and input crank.

3) The foot clears the ground as it recycles in between stance phases.
4) A simple geometric adjustment allows for an efficient, low-powered walking mode.

To design this, we consider a single degree-of-freedom planar linkage with an input crank and an output path. The constrained motion between the crank and path (Fig. 1) might be defined by a six-bar linkage (Fig. 2). The constrained motion illustrated in Fig. 1 achieves the first three required behaviors. The second and third behaviors follow from the fact that the path is specified as a closed loop with a linear ground contact section and an arced ground clearance section. The first required behavior follows from the coordination of path arc length $s$ and crank angle $\phi$. The derivative of $\phi = f(s)$, shown in Fig. 1b, is what is known as mechanical advantage. Mechanical advantage defines the ratio of the output force $F$ acting tangentially to the foot path and the input torque $T$ acting on the crank. This follows from the power balance of an ideal mechanism,

$$T\dot{\phi} = F\dot{s}. \tag{1}$$

The input torque is modelled by a DC motor supplied with a constant voltage connected mechanically in series with a torsion spring acting on the input crank. The output force acts to do work on a load. The dynamics of this DC motor powered model are compactly represented in conceptual blocks in Fig. 3.

A motor stall torque of 0.33 Nm and free-running speed of 11.5 rad/s was specified according to a commercially off-the-shelf component (Pololu 3079). A spring stiffness of

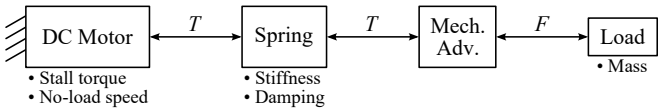


Fig. 3. A simple model of a DC motor transmitting torque through a spring in series to a mechanical advantage transformation that defines the ratio between torque and the force acting on the load. Model parameters are given as bullet points.

0.14 Nm/rad and damping of 0.0005 Nm/(rad/s) follows that of a 0.014 mm diameter cylindrical cut of natural rubber latex. The proposed mass is 249 grams. Simulation of Fig. 3 indicates the mechanical power acting on the mass to be 2.88 W. As the maximum power output of the motor is 0.95 W, this indicates a power modulation factor of 3.03.

It is assumed that moving links, which are not yet known, have no inertia. As well, the motor and mechanism are fixed and accelerating a load on a horizontal plane without friction. The dynamics of the physical model represented by the conceptual diagram of 3 were solved with a numerical differential equation solver available in Mathematica.

The feature of adjustability is not encapsulated in the task specification shown in Fig. 1. Instead, this requirement is implemented in a post process.

The task specified in Fig. 1 was constructed by clicking points on a computer screen, then interpolating them with Fourier series. The mechanical advantage (MA) plot (Fig. 1b) follows the principles outlined in [13] to create a low MA region where spring energy is accumulated followed by a rise in MA to release this energy. This characteristic creates the power modulating behavior.

### *B. Computational Synthesis*

As illustrated in Fig. 2, the six-bar linkage topology might accomplish the desired behaviors. Many different synthesis problems related to the four-bar have been formulated and solved for their complete solution sets [14]. Here we refer to complete solution sets as all of the isolated roots of square systems of dimensional synthesis equations.

Generally, four-bar motions are basic (sextic plane curves [15]) and the number of dimensional design parameters available to adjust is limited. Six-bar linkages offer a huge increase in design space complexity. On one hand, this makes design harder since more dimensional design parameters are embodied in higher degree design equations. On the other hand, this increase in design space offers more candidate solutions and six-bars generally accomplish more complex motions (degree 16 plane curves [16]).

We select a Stephenson II linkage (shown in Fig. 2) to perform the required task. Eight coordinated coupler points and crank angles were selected from Fig. 1 to approximate the required motion. The synthesis of a mechanism to generate a specified path coordinated with crank input angle is referred to as *timed curve generation*. A set of design equations was formulated by summing vectors of mechanism loops and coupler points using isotropic coordinates [17], similar to the approach given in [18].

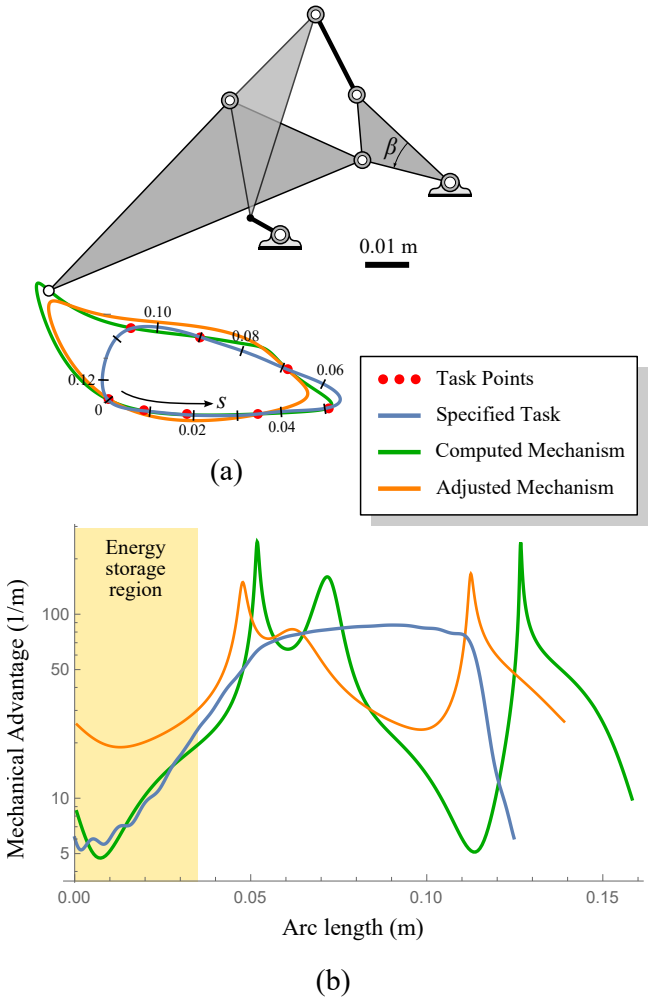


Fig. 4. (a) A result from the computational design routine that was chosen to be built and tested. (b) Mechanical advantage of the synthesized linkage is compared to the task specification and the adjusted mechanism.

The complete set of isolated roots for this square system of equations corresponding to Stephenson II timed curve generation has never been obtained before. We obtain all these roots for the first time using the Finite Root Generation (FRG) method [19]. FRG found 1,529,788 solutions of a numerically generic version of these synthesis equations. FRG estimated this to be 99.0% of finite roots. The algorithm ran for 24 hours on a laptop GPU (MSI GS70, GeForce GTX 970M). FRG's numerically generic results were used to compute a parameter homotopy [20] to find 3764 mechanism solutions for our specific synthesis system. The mechanism solution selected to prototype and test is shown in Fig. 4 alongside its task objective.

Note that the computational synthesis approach outlined above is optimization-free. Design requirements were mapped into a system of nonlinear kinematic equations which were directly solved by obtaining all isolated roots to a square system of synthesis equations.

To interpret Fig. 4b, note that when mechanical advantage is nearly zero, the mechanism is very close to locking up. That is, the load on the end-effector point results in a large torque at the input. In contrast, at the peaks of mechanical advantage, a small input torque can easily handle loads at the output, resulting in smooth operation. It was an undesired consequence that our designed mechanism possessed a second dip in mechanical advantage beyond the energy storage region. However, since this region occurs when the foot point is in the air under no load, the design remains functional.

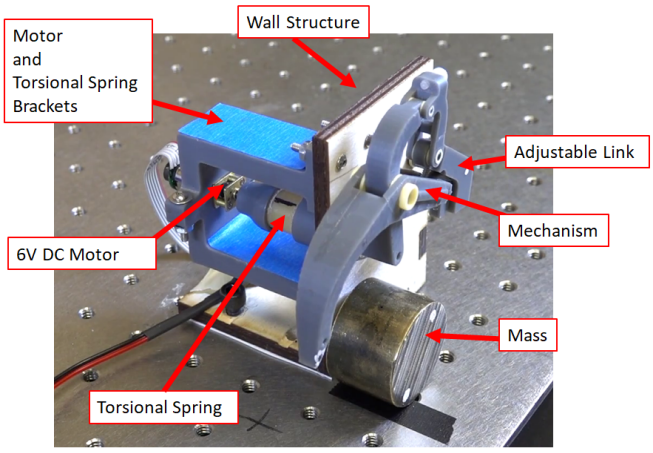


Fig. 5. The prototype mechanism set up to push a cylindrical weight.

### C. Adjustability

In order to realize the fourth required behavior, individual dimensions were modified, and changes in mechanical advantage and foot path shape were noted. The angle $\beta$ shown in Fig. 4a was found to be a convenient dimension to adjust. Decreasing it by 4° quadruples mechanical advantage at the energy storage region, greatly reducing the power modulation factor. This adjustment is useful if efficient low-powered walking is desired.

## III. METHODS

### A. Prototyping

The mechanism links were designed in Solidworks and printed using a Form2 3D printer. The prototype is shown in Fig. 5, situated in a test apparatus. Joints were designed to be in double shear and attach to a plywood structure. Igus flange bearings were used at the joints. The adjustable link discussed in the previous section is shown in Fig. 6. The angle $\beta$ maybe be modified by turning two screws.

The spring is a 14 mm diameter cylindrical cut of latex acting in series with the motor. It is connected between the motor shaft and the crank of the mechanism. To test the spring stiffness, the spring was installed vertically between two brackets and twisted by applying a force from 0 to 8.8 N in increments of 2.2 N at 0.043 m on a lever arm. The torsional spring stiffness was determined to be about 0.14 Nm/rad. A Pololu 6V DC motor was used to drive the mechanism. This motor has a 298:1 gear ratio, a no-load speed of 11.5 rad/s, and stall torque of 0.33 Nm.

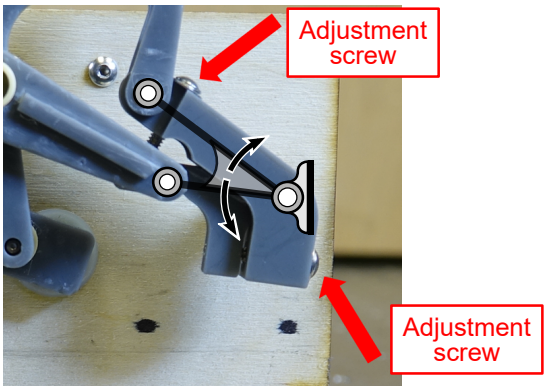


Fig. 6. An adjustable angle link that transitions the mechanism between high-power and low-power modes.

### B. Testing Procedures

Two tests were conducted on the leg mechanism. The set up for the first is displayed in Fig. 5. The mechanism was secured to a table and a 0.249 kg cylindrical weight was staged below its foot. Then 6V were applied to the motor from a bench top power supply so that the mechanism would kick the weight. The resulting motion of the weight was measured to determine the leg's energetic output. As well, current readings were logged during this kicking motion to determine the operating condition of the motor.

For the second test, lightweight foam wheels were attached to the mounting structure of the leg mechanism to create a cart. The cart rolled along a smooth, level table. The cart was propelled by the leg itself as it pushed on the teeth of a plywood sawtooth track. To minimize out-of-plane roll motions, a 0.3 m long carbon fiber rod was attached to the cart orthogonal to the mechanism's plane of motion. These efforts served to planarize the propulsive of path of the leg and cart. The mass of the moving cart was 0.140 kg.

A Sony DSC-RX10M3 captured the motion of the leg mechanism during the load pushing test as well as traversing the sawtooth track test. The videos were recorded at 960 frames per second. White and black dots were painted on the foot of the mechanism, the plywood support structure, and the flat side of the cylindrical weight. These points were tracked using Tracker Video Analysis software to determine the position and velocity of the mechanism and mass. Current sensing was accomplished with a ACS712. High speed video and sensor recordings were synchronized by blinking an LED in sight of the camera

## IV. RESULTS

Characteristic performance of the mechanism is shown in Fig. 7. During a typical cycle, the angular velocity of the input crank slows from 9 rad/s to about 0.5 rad/s as it enters the energy storage region of low mechanism advantage. Note that rotation of the input never actually halts. At this point, motor current rises from roughly 20% of stall current (1.5 A) to 87% of stall current as torque increases in the spring. Upon exiting the energy storage region, the mass is rapidly accelerated by a power greater than three times the motor's limit.

Fig. 7 displays synchronized high-speed video and current recordings. The angular velocity of the crank was measured from the high speed video. Seven trials are displayed. The trial shown in blue correlates to the video stills displayed above. Precise timing of the video stills is indicated with orange triangles.

The advantage of this mechanism is to achieve higher powered motions. We argue that this primitive extends the set of viable footholds. However, the motor operates near stall where it is less efficient. In the case that an extended set of footholds is not necessary, we offer a single dimensional adjustment to transition to a low-power mode. However, the means for automatic adjustment of this dimension is left out of scope for this paper. In the proceeding subsections, we compare low-power to high-power modes of the mechanism.

### A. Energizing a Rolling Mass from a Fixed Mechanism

The mechanism was set up to push the cylindrical weight in both high-powered and low-powered modes. To transition between modes, the screws shown in Fig. 6 were adjusted. Energetic output was determined from translation and rotation of the cylindrical mass measured from high-speed video at the moment of losing contact with the mechanism's foot.

Five trials were conducted for each the high- and low-powered modes. The high-powered mode accelerated the mass to an average translational speed of 0.688 m/s with a standard deviation (S.D.) of 0.00860 m/s The low-powered mode accelerated the mass to 0.368 m/s with an S.D. of 0.00896 m/s. Accounting for the kinetic energy of the cylinder, the high-power case energized it to 0.0663 J with an S.D. of 0.00180 J, while the low-power case energized it to 0.0254 J with an S.D. of 0.00127 J. Transitioning between and high- and low-powered modes adjusted energetic output by over a factor of two. Trial to trial testing was consistent.

### B. Traversing Terrain

Both high- and low-powered modes of our mechanism were tested for cyclically propelling itself forward. In this case, the leg was attached to a rolling cart constrained from lateral movement. The leg hung out above the cart over a sawtooth terrain, seen in Fig. 8. Inertia was balanced by attaching a long carbon fiber rod on the back of the cart perpendicular to the mechanism's plane of motion. The sawtooth terrain pattern eliminated friction as a source of variation in this experiment. Note that this prototype without modification would be limited by friction when traversing more realistic terrain.

Fig. 8 displays the trace of the mechanism's foot from frame to frame tracking for a single trial of high- and low-power modes. Traces occurred over a 3 second timespan. High power mode allowed sequential footholds to be farther apart at the cost of efficiency.

Performance between these two design modes can be characterized by work per step. Fig. 9 plots linear horizontal velocity of the cart as a function of time for both design

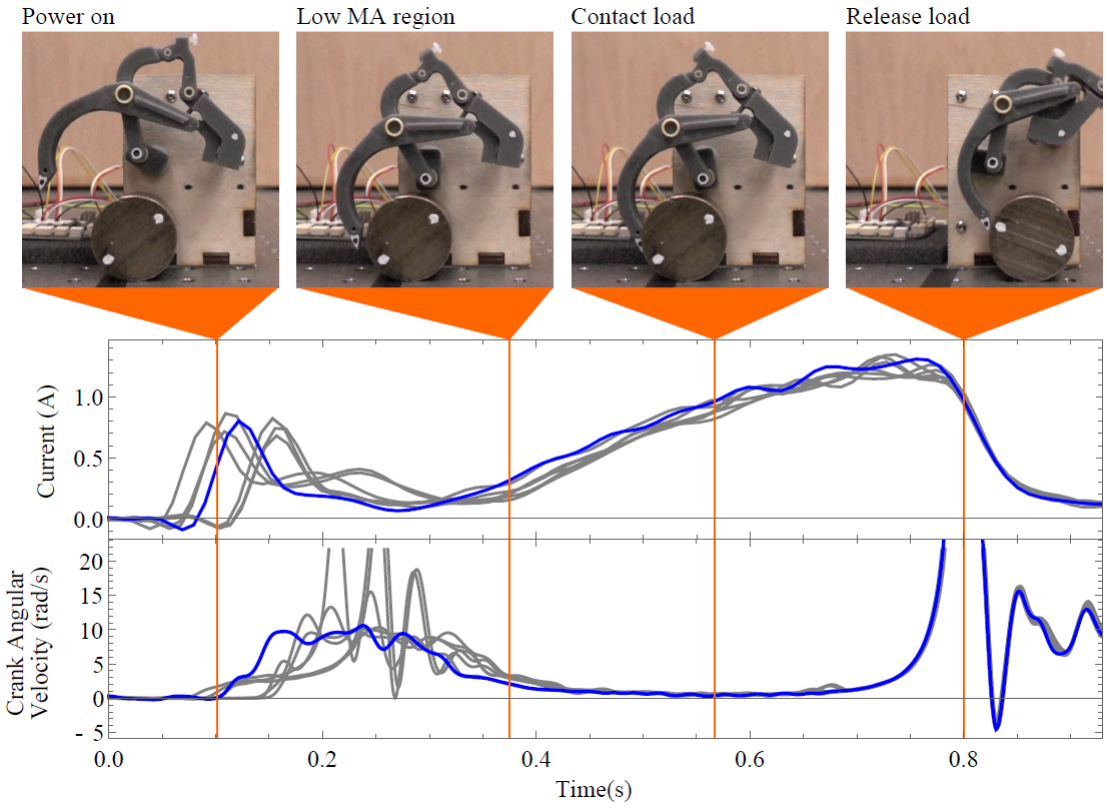


Fig. 7. Current draw and crank rotation as the mechanism pushes a weight through its energy storage region.

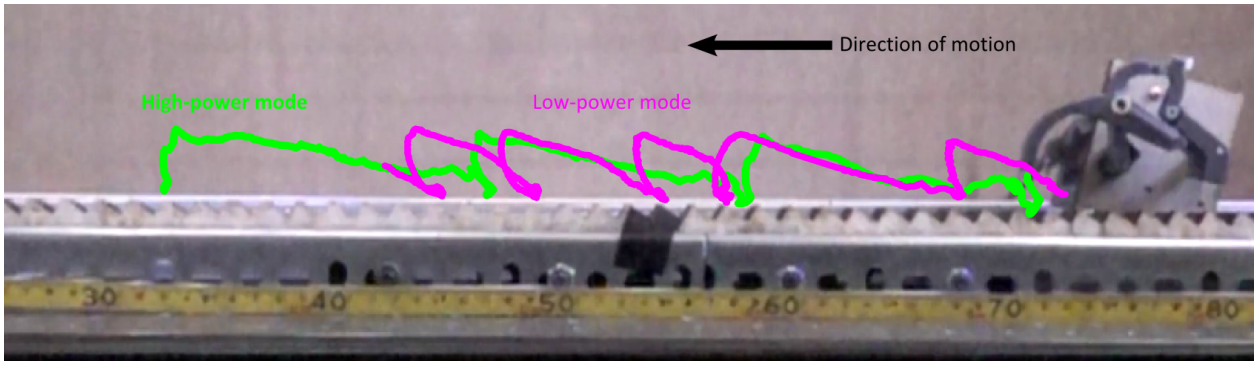


Fig. 8. The mechanism was attached to a cart, then propelled itself over a sawtooth terrain to understand its cyclic work output per step. Lines trace the motion of the foot over 3 seconds of high speed footage. The sawtooth pattern was specified to eliminate the confounding effects of friction.

modes. The energetic output of individual stance phases are clearly identified as the peaks in this graph. For each peak (i.e. for each step), we can compute the change in kinetic energy of the cart as the useful work performed in a single step. Work output for individual steps is illustrated in Fig. 9 as rectangular bars underlaying each velocity peak. For this trial, the high-power mode achieved over four times more work per step than the low-power mode.

## V. CONCLUSIONS

This paper presented a novel design for a leg mechanism suitable for development into a running robot. We delineated design requirements and connected geometric constraints to dynamic behaviors. The required behaviors were distilled into a large system of equations from which all isolated roots were obtained using the Finite Root Generation method. This paper investigated a single mechanism output by our computational routine. This mechanism instantiated so-called power modulating mechanics to surpass actuator power limits. The focus on power is motivated by accessing new footholds through leaping or bounding, tasks which are fundamentally limited by power output during a short stance phase. We surmise that designing a terrestrial robot capable of switching in and out of high-powered mechanics would be useful. Therefore, we have identified a route by which our presented mechanism might be adjusted into a low-power efficient mode.

Basic experiments were conducted on the newly intro-

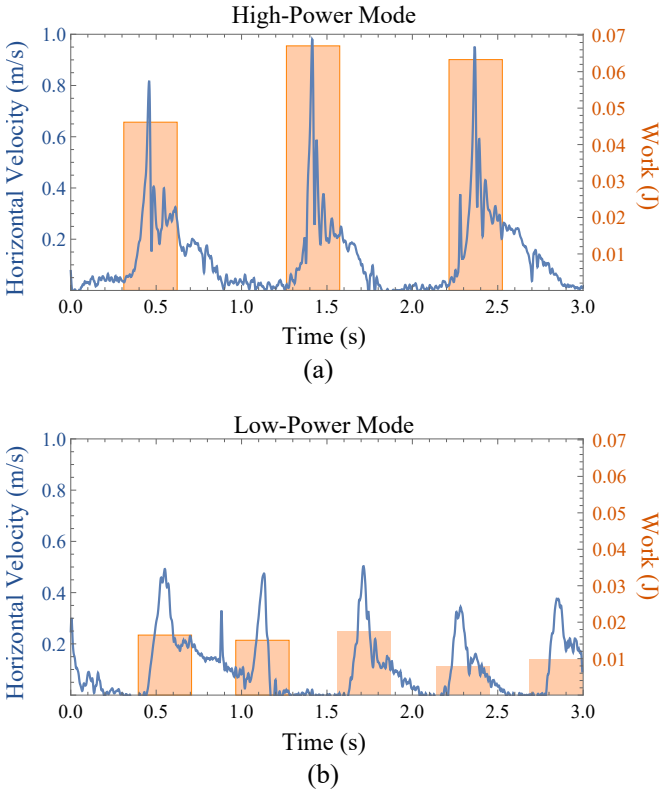


Fig. 9. Velocity of the cart as a function of time and step to step work output for (a) high-power and (b) low-power modes.

duced design. The energetic output of moving inertial loads was characterized by first securing the mechanism and powering an external mass, then allowing the mechanism to cyclically propel itself in a control manner. Finally, we related the work per step generated during high- and low-power mechanism modes to the ability of a leg to sequentially access more distant footholds.

## ACKNOWLEDGMENT

The authors would like to thank Justin Yim, Carlos Casarez, and Ethan Schaler for their valuable insights and conversations. We also gratefully acknowledge the support of the National Science Foundation through award CMMI-1636302. Any opinions, findings, and conclusions or recommendations expressed in this material are those of the authors and do not necessarily reflect the views of the National Science Foundation.

## REFERENCES

[1] Haldane, D. W., Plecnik, M. M., Yim, J. K., & Fearing, R. S. (2016). Robotic vertical jumping agility via series-elastic power modulation. Science Robotics, 1(1), eaag2048.

[2] Plecnik, M. M., Haldane, D. W., Yim, J. K., & Fearing, R. S. (2017). Design exploration and kinematic tuning of a power modulating jumping monopod. Journal of Mechanisms and Robotics, 9(1), 011009.

[3] Wensing, P. M., Wang, A., Seok, S., Otten, D., Lang, J., & Kim, S. (2017). Proprioceptive actuator design in the MIT cheetah: Impact mitigation and high-bandwidth physical interaction for dynamic legged robots. IEEE Transactions on Robotics, 33(3), 509–522.

[4] Kenneally, G. D., De, A., & Koditschek, D. E. (2016). Design Principles for a Family of Direct-Drive Legged Robots. IEEE Robotics and Automation Letters, 1(2), 900–907.

[5] Haldane, D. W., & Fearing, R. S. (2015). Running beyond the bio-inspired regime. In the 2015 IEEE International Conference on Robotics and Automation, pp. 4539–4546.

[6] Jung, G. P., Casarez, C. S., Jung, S. P., Fearing, R. S., & Cho, K. J. (2016). An integrated jumping-crawling robot using height-adjustable jumping module. In the 2016 IEEE International Conference on Robotics and Automation, pp. 4680–4685).

[7] Casarez, C. S., & Fearing, R. S. (2016). Step climbing cooperation primitives for legged robots with a reversible connection. In the 2016 IEEE International Conference on Robotics and Automation, pp. 3791–3798.

[8] Paluska, D., & Herr, H. (2006). The effect of series elasticity on actuator power and work output: Implications for robotic and prosthetic joint design. Robotics and Autonomous Systems, 54(8), 667–673.

[9] De, A., & Koditschek, D. E. (2015). Parallel composition of templates for tail-energized planar hopping. In the 2015 IEEE International Conference on Robotics and Automation, pp. 4562-4569.

[10] Saranli, U., Buehler, M., & Koditschek, D. E. (2001). RHex: A simple and highly mobile hexapod robot. The International Journal of Robotics Research, 20(7), 616–631.

[11] Yesilevskiy, Y., Xi, W., & Remy, C. D. (2015, May). A comparison of series and parallel elasticity in a monoped hopper. In the 2015 IEEE International Conference on Robotics and Automation, pp. 1036–1041.

[12] Plecnik, M. M., & Fearing, R. S. (2017). Finding only finite roots to large kinematic synthesis systems. Journal of Mechanisms and Robotics, 9(2), 021005.

[13] Haldane, D. W., Plecnik, M., Yim, J. K., & Fearing, R. S. (2016). A power modulating leg mechanism for monopedal hopping. In the 2016 IEEE/RSJ International Conference on Intelligent Robots and Systems, pp. 4757–4764.

[14] Brake, D. A., Hauenstein, J. D., Murray, A. P., Myszka, D. H., & Wampler, C. W. (2016). The complete solution of Alt-Burmester synthesis problems for four-bar linkages. Journal of Mechanisms and Robotics, 8(4), 041018.

[15] Hartenberg, R. S., & Denavit, J. (1964). Kinematic synthesis of linkages. McGraw-Hill.

[16] Primrose, E. J. F., Freudenstein, F., & Roth, B. (1967). Six-bar motion II. The Stephenson-1 and Stephenson-2 mechanisms. Archive for Rational Mechanics and Analysis, 24(1), 42–72.

[17] Wampler, C. W. (1996). Isotropic coordinates, circularity, and Bezout numbers: planar kinematics from a new perspective. In the 1996 ASME Design Technical Conference, Paper No. 96-DETC/MECH-1210.

[18] Plecnik, M. M., & McCarthy, J. M., (2016). "Computational Design of Stephenson II Six-bar Function Generators for 11 Accuracy Points," Journal of Mechanisms and Robotics, JMR-15-1055, 8(1): 011017

[19] Plecnik, M. M., & Fearing, R. S. (2017). A study on finding finite roots for kinematic synthesis. In the 2017 ASME International Design Engineering Technical Conferences & Computers and Information in Engineering Conference, Paper No. IDETC2017-68341.

[20] Morgan, A. P., & Sommese, A. J. (1989). Coefficient-parameter polynomial continuation. Applied Mathematics and Computation, 29(2), 123–160.